Molecular dynamics simulation comparison of atomic scale intermixing at the amorphous Al_2O_3/semiconductor interface for a-Al_2O_3/Ge, a-Al_2O_3/InGaAs, and a-Al_2O_3/InAlAs/InGaAs

Evgueni A. Chagarov *, Andrew C. Kummel

Department of Chemistry and Biochemistry, University of California, San Diego, La Jolla, CA 92093, United States

A B S T R A C T

The structural properties of a-Al_2O_3/Ge, a-Al_2O_3/$In_{0.5}Ga_{0.5}As$ and a-Al_2O_3/$In_{0.5}Al_{0.5}As$/InGaAs interfaces were investigated by density-functional theory (DFT) molecular dynamics (MD) simulations. Realistic a-Al_2O_3 samples were generated using a hybrid classical-DFT MD "melt and quench" approach. The interfaces were formed by annealing at 700 K/800 K and 1100 K with subsequent cooling and relaxation. The a-Al_2O_3/Ge interface demonstrates pronounced interface intermixing and interface bonding exclusively through Al–O–Ge bonds generating high interface polarity. In contrast, the a-Al_2O_3/InGaAs interface has no intermixing, Al–As and O–In/Ga bonding, low interface polarity due to nearly compensating interface dipoles, and low substrate deformation. The a-Al_2O_3/InAlAs interface demonstrated mild intermixing with some substrate Al atoms being adsorbed into the oxide, mixed Al–As/O and O–Al/In bonding, medium interface polarity, and medium substrate deformation. The simulated results demonstrate strong correlation to experimental measurements and illustrate the role of weak bonding in generating an unpinned interface for metal oxide/semiconductor interfaces.

1. Introduction

The rapid scaling of complementary metal-oxide–semiconductor (CMOS) technology requires substituting the traditional gate oxide, SiO_2, with high-κ dielectrics, which can maintain the same capacitance with much lower leakage current. Amorphous alumina is one of the candidates for such high-κ gate oxide materials. It is widely used for gate dielectrics and tunneling barriers due to its insulating properties, thermal and chemical stability, and strong adhesion in hetero-junctions. Ge and InGaAs offer significantly higher mobility than silicon and are being extensively investigated for p- and n-channel high-κ MOSFETs, respectively [1–3]. InAlAs is a possible confinement layer in InGaAs MOSFET's.

Although there are previously reported density-functional theory simulations of high-κ oxide–semiconductor interfaces, to our knowledge, there are only few reports on amorphous oxide bonding [4–9]. Amorphous oxide–semiconductor interfaces are likely to be superior to crystalline oxide–semiconductor interfaces because the large differences in unit cell sizes prevent growth of crystalline oxides on semiconductors without a high density of defects. Despite its chemical composition similarity to crystalline phase, amorphous Al_2O_3 demonstrates quite different microstructure,

coordination distribution, and atomistic chemical environment compared to its crystalline polymorph.

While many previously reported simulations of oxide–semiconductor interfaces were limited to artificially formed structures relaxed at 0 K, this study employs DFT molecular dynamics (DFT-MD) at finite temperatures thereby providing the system with enough freedom to naturally evolve over time into the most realistic state.

2. Generation of amorphous Al_2O_3 samples

The realistic amorphous Al_2O_3 samples matching Ge(1 0 0), $In_{0.5}Ga_{0.5}As$ and $In_{0.5}Al_{0.5}As$ substrate surface areas were generated by a hybrid classical-DFT MD "melt and quench" approach [7,8,10]. The amorphous sample quality was verified via the radial-distribution function (RDF) main peak positions and full widths at half maximum (FWHM), average nearest neighbor numbers, nearest neighbor distributions, calculated neutron scattering static structural factor, and DFT calculated band gap demonstrating good correlation to simulated and experimental reference properties [11–13]. The generation of a-Al_2O_3 for the Ge(1 0 0)(2 × 1) surface cross-sectional area was described in detail elsewhere [8,10].

A separate a-Al_2O_3 sample was generated with DFT-MD to match the InGaAs and InAlAs substrate surface area. This a-Al_2O_3 sample was classically annealed at low (∼0.9 g/cm³) density at

5000 K for 250 ps, rescaled to normal classical a-Al_2O_3 density of 3.20 g/cm^3 and annealed at 5000 K for 400 ps, linearly cooled to RT for 100 ps, and thermally equilibrated at RT for 120 ps, demonstrating properties very close to a published reference classical sample [11].

Amorphous Al_2O_3 can be stable over a wide range of densities. Experimental measurements report stable amorphous Al_2O_3 structures with a 3.05–3.40 g/cm^3 density range [14,15], while classical and DFT computer simulations demonstrate successful generation at 3.0–3.3 g/cm^3 [11,13,16]. The classical density of the a-Al_2O_3 sample in this study was chosen to be consistent with previous classical simulations of a-Al_2O_3 that correlated well with experimental properties [11,12]. The selected classical a-Al_2O_3 sample was rescaled to equilibrium DFT density of 3.26 g/cm^3, DFT annealed at 1400 K for 1000 fs, linearly cooled to 0 K for 200 fs and relaxed below 0.01 eV/Å force tolerance level. The ratio of the classical and DFT a-Al_2O_3 density was determined by DFT annealing of a separate classical a-Al_2O_3 sample and relaxation at variable volume. Table 1 presents coordination distribution of our classically annealed sample for InGaAs and InAlAs substrates vs. reference classical sample distribution demonstrating excellent correlation [11]. The bulk a-Al_2O_3 sample for InAlAs/InGaAs substrate demonstrates defect-free bandgap of ~3.7 eV, agreeing well with a bandgap of 3.8 eV for our bulk a-Al_2O_3 sample made for Ge substrate size [8], and the previously reported value of 3.77 eV [13].

3. Substrates

The 64-atom Ge(1 0 0)(2 × 1) substrate was formed from a 2 × 2 × 2 Ge supercell with the DFT optimized lattice constant. The bottom three layers were fixed in the bulk positions and passivated by H atoms. The rest of the slab was relaxed below the 0.01 eV/Å force tolerance level to form the Ge(1 0 0) (2 × 1) surface reconstruction with a ~11.58 × 11.58 × 10.4 Å slab size.

The $In_{0.5}Ga_{0.5}As$ substrate was relaxed forming a 4 × 2 surface reconstruction with the 3 bottom atomic layers fixed in their bulk positions. The bottom layer As atoms were passivated by H atoms with fractional 3/4 |e| charge to mimic continuous bulk according to Ref. [17]. The preliminary $In_{0.5}Ga_{0.5}As$ bulk unitcell was formed from GaAs unitcell by substituting half of Ga atoms by In following a checkerboard pattern and DFT optimizing the lattice constant of the alloy to the equilibrium value.

For modeling bonding to $In_{0.5}Al_{0.5}As$, a heterostructure was used consisting of 6 bottom layer of $In_{0.5}Ga_{0.5}As$ and 7 top layers of $In_{0.5}Al_{0.5}As$. The $In_{0.5}Al_{0.5}As$ bulk unit cell was formed in the similar manner from GaAs unit cell by substituting half of the Ga by Al and the other half by In following a checkerboard pattern with subsequent DFT optimization of the lattice constant. The DFT optimized lattice constants of the relaxed InAlAs and InGaAs unitcells differ by 0.3%, and in the stack they share the same cross-sectional area without creating significant lateral stresses. For the InAlAs/InGaAs substrate, the bottom As atoms were passivated by 3/4 |e| H atoms [17].

The DFT calculations of InGaAs and InAlAs bulk samples with the PBE functional produce DOS curves with zero bandgap for InGaAs and a clear band-gap for InAlAs of 0.47 eV. The DFT of the clean InGaAs(1 0 0)-(4 × 2) slab shows a bandgap of about 0.4 eV for the lowest energy 4 × 2 reconstruction. This is the most relevant bandgap for comparison to the oxide/semiconductor interface structures. The bandgap of the relaxed a-Al_2O_3/InGaAs(1 0 0) interface derived from the DOS calculation demonstrates clear non-zero bandgap and will be discussed later. The InGaAs and InAlAs bandgaps can be "expanded" by applying much more computationally expensive hybrid functionals, like PBE0 or similar, which add exact exchange interaction into the model.

To satisfy periodic boundary conditions, the sizes of the DFT annealed and relaxed a-Al_2O_3 samples perfectly match the DFT optimized Ge(1 0 0)(2 × 1), InGaAs, and InAlAs/InGaAs substrate surface areas.

4. Computational details

Classical MD simulations were performed by a Large-Scale Atomic/Molecular Massively Parallel Simulator (LAMMPS) [18], expanded by well-tested empirical potential for Al_2O_3 [19]. All DFT simulations were performed with the Vienna Ab-Initio Simulation Package (VASP) [20,21] using projector augmented-wave (PAW) pseudopotentials (PP) [22,23] and PBE (Perdew–Burke–Ernzerhof) exchange–correlation functional [24,25]. The choice of PBE functional and PAW PP's was validated by parametrization runs demonstrating good reproducibility of experimental lattice constants, bulk moduli, and formation energies for bulk crystalline Al_2O_3, Al, Ge, GaAs, and InAs.

5. Stack formation and annealing procedure

The DFT annealed a-Al_2O_3 samples were cleaved in the X–Y plane parallel to the interface breaking periodic boundary conditions by introducing ~12 Å of vacuum over the samples. Since InGaAs(1 0 0)-(4 × 2) and InAlAs(1 0 0)-(4 × 2) experimental surfaces have a row-trough structure, the corresponding oxide sample was cleaved to form a groove of 7.5 Å × 1.7 Å to match the substrate row/trough topography. The cleavage planes of the a-Al_2O_3 samples for the three substrates were chosen to get a roughly equal number of aluminum and oxygen atoms on the oxide surface in contact with the substrates. The corresponding a-Al_2O_3 sample was placed on the relaxed Ge, InGaAs, or InAlAs/InGaAs substrates at a height such that the initial interfacial bond lengths were equal to approximately 0.5–0.75 of their empirical equilibrium distance. The dangling bonds on the oxide upper surface were passivated by H atoms having ~12 Å of vacuum to avoid spurious interactions through periodic boundary conditions. The oxide sample was not relaxed after surface cleavage prior to stacking on Ge, InGaAs, or InAlAs/InGaAs in order to provide a chemically reactive surface with dangling bonds in contact with the substrate, thereby having closer correlation to real deposition conditions. On average, the initial interfacial bond lengths were about 0.70–0.75 of the equilibrium distance. There were values close to 0.5–0.6 for a few bonds since the horizontal cut of amorphous sample usually produces a very non-planar oxide surface topography which creates a corrugated interface to the planar parts of semiconductor surface. The initial interfacial distance was chosen to be on the repulsive rather than on attractive portion of the potential to prevent the oxide from relaxing into an oxide/vacuum interface structure on the fresh-cut surface. By being on the repulsive portion of the potential, the oxide dangling bonds are preserved which are in contact

Table 1
Nearest neighbor distribution of our classical a-Al_2O_3 sample for InGaAs and InAlAs substrates vs. classical sample of Ref. [11]. Cutoff radius-2.2 A.

Nearest neighbor distribution	O(2)	O(3)	O(4)	Al(3)	Al(4)	Al(5)	Al(6)
Our sample	18%	79%	3%	0.0%	75%	23%	2.0%
Ref. [11]	20%	78%	2%	0.3%	76%	22%	1.7%

with the semiconductor surface, mimicking the physics during real oxide deposition. Furthermore, the initial partial relaxation with a fixed semiconductor substrate quickly equilibrates the interfacial bond lengths. In contrast to other published DFT-MD oxide/semiconductor studies, stacks were employed with one oxide/semiconductor interface and a vacuum spacer since the supercell model with two oxide/semiconductor interfaces and no vacuum could unphysically restrict atomic migration to/from the oxide/semiconductor interface in the thin oxide film ($\sim$10 Å). More importantly, the presence of a vacuum spacer over the oxide provides complete relaxation of the interfacial oxide–semiconductor height and any possible residual stresses in the system induced by mutual bonding. To compensate for spurious electric field induced by PBC for this type of system, a dipole correction was applied [20,21,26].

After initial formation of the a-Al_2O_3/semiconductor stacks, they were annealed according to the following general procedure. Initially, the whole semiconductor substrate was fixed in space while the oxide was partially relaxed for $\sim$20–30 conjugate-gradient (CG) relaxation steps. The duration of this initial relaxation was systematically determined by performing longer ($\sim$150 CG steps) relaxation runs, which demonstrated that $\sim$20–30 CG steps were sufficient to reach the optimal interface height, releasing initial artificial interface stresses and allowing the oxide to conform to the non-planar reconstructed substrate topography. After the initial partial relaxation with a frozen semiconductor substrate, the substrate atoms were unfixed except for the three bottom layers, and the whole system was annealed at a fixed annealing temperature for 1000 fs with 1.0 fs timesteps, cooled to 0 K over 200 fs, and finally relaxed below a 0.05 eV/Å force tolerance level. To investigate the effect of temperature, stacks were annealed at several temperatures. The lower DFT annealing temperature value matched typical temperatures for oxide deposition and post-deposition annealing (PDA), and the higher DFT annealing temperature

value was intended to effectively increase the simulated timescale through accelerated atomic kinetics. Due to the high computational cost of performing DFT MD runs ($\sim$250 atoms and $\sim$2500 CG/MD steps) and the large PBC box size, the initial relaxation, annealing, cooling and final relaxation were performed with a 2 K-point irreducible set. After the final relaxation, the K-point set was expanded to $3 \times 3 \times 1$ (for a-Al_2O_3/Ge) or $2 \times 4 \times 1$ (for a-Al_2O_3/InGaAs and a-Al_2O_3/InAlAs/InGaAs), and the system was refined by another relaxation run. Although expansion of the K-point set had no visible effect on the system geometry and required only $\sim$30–50 CG steps to relax below the 0.05 eV/Å force tolerance level, it could improve the electronic structure.

6. Results and discussion

6.1. Bonding structure

The a-Al_2O_3/Ge(1 0 0)(2 × 1) interface was annealed at 700 K and 1100 K. In both cases, the interfaces demonstrate very pronounced chemical segregation with oxygen atoms migrating to the semiconductor interface and Al atoms migrating into the bulk oxide resulting in interfacial bonding exclusively through Al–O–Ge bonds with no or very few O–Al–Ge bonds (Fig. 1) [7]. Increasing the interfacial DFT annealing temperature from 700 K to 1100 K had no effect on the interface chemical migration. The interface segregation was very fast, occurring during the first $\sim$100 fs (10% of the whole annealing time), proving that the DFT timescale is sufficient to observe this phenomenon (Fig. 1). The oxygen enrichment of a-Al_2O_3/Ge interface was very similar to an oxygen enrichment of a vacuum/a-Al_2O_3 interface [8,16,27,28].

The a-Al_2O_3/$In_{0.5}Ga_{0.5}$As(1 0 0)-4 × 2 interfaces were annealed at 800 K both in the one-interface (Fig. 2) and the two-interface
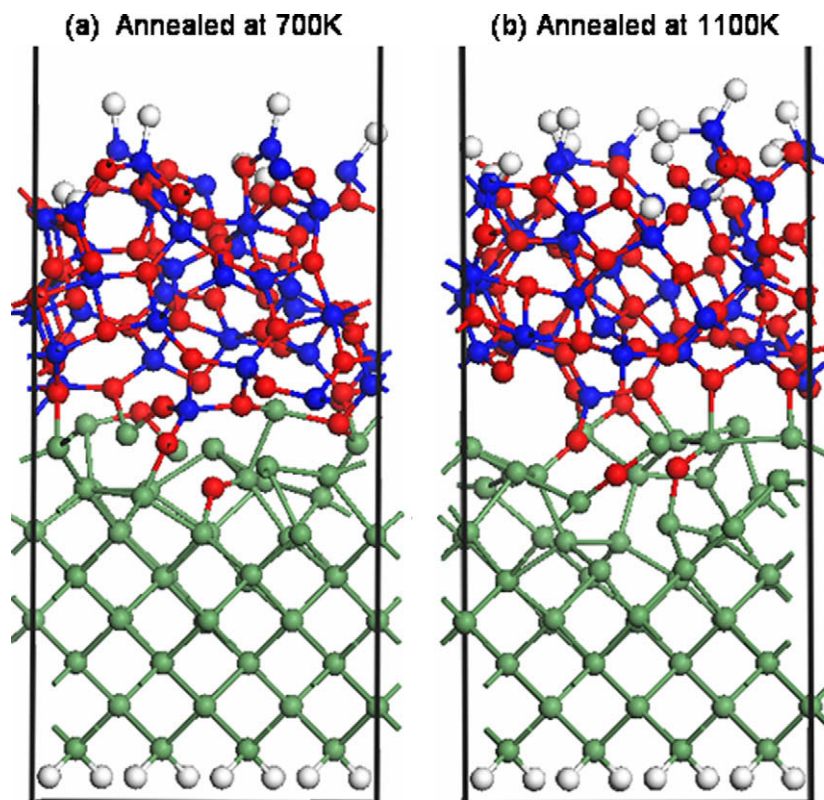
Fig. 1. a-Al_2O_3/Ge(1 0 0)(2 × 1) stacks after final relaxation: (a) annealed at 700 K and (b) annealed at 1100 K. Ge-green, Al-blue, O-red, H-white. (For interpretation of the references to colour in this figure legend, the reader is referred to the web version of this article.)
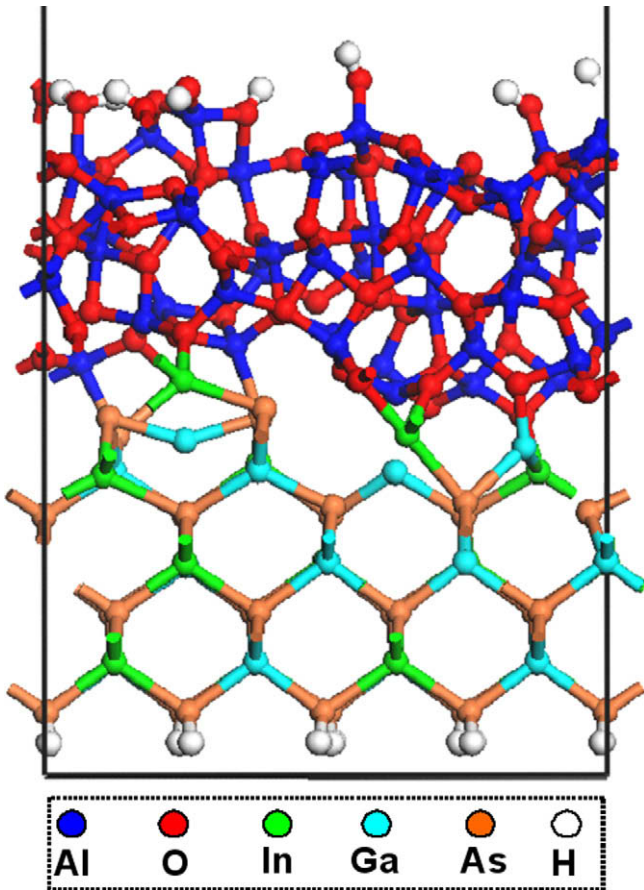
Fig. 2. a-Al$_2$O$_3$/InGaAs one-interface stack after final relaxation. Annealing temperature is 800 K.

tween the oxide and the semiconductor is a weak covalent bonding so any stresses at high temperature can induce an irreversible delamination in the relatively small simulation box with periodic boundary conditions employed in these studies. It is noted that this would not occur in real experimental systems with much bigger system sizes containing step-edges.

Three typical causes of midgap states are As–O bond formation, interface intermixing, and disruption of the substrate lattice to form new dangling bonds [29]; the DFT model of the ideal a-Al$_2$O$_3$/In$_{0.5}$Ga$_{0.5}$As(1 0 0)-(4 × 2) interface (Fig. 2) shows the absence of all three of these phenomena.

The a-Al$_2$O$_3$/InAlAs interface of the a-Al$_2$O$_3$/InAlAs/InGaAs stack demonstrates a low density of Al–O, Al–As, and O–In bonds with moderately compensating bond-dipoles (Fig. 3). During annealing, a few Al atoms are pulled out of InAlAs into the oxide forming single Al–In bonds, which look like irregularities and are a direct result of the interface intermixing.

6.2. Substrate deformation

The interface intermixing and deformation can have significant adverse effects on interface physical and electrical properties, such as decreasing of carrier mobility, creation of midgap states which pin the interface, and formation of interfacial layer. To quantify

designs (EPAPS Fig. 1). The systems for both designs demonstrated similar interface bonding structures formed by polar As–Al bonds and In/Ga–O bonds of opposite dipole direction and demonstrated the absence of O–As bonds.

The a-Al$_2$O$_3$/InGaAs stack (Fig. 2) had several dangling bonds (unpassivated states) at the a-Al$_2$O$_3$/vacuum interface (upper oxide surface), which formed states in the band gap region of the total DOS. The pinning states were localized at the under-coordinated Al atoms having two bonds to O's and one to H. In amorphous bulk a-Al$_2$O$_3$ oxide, Al has predominantly 4 bonds to O. It is noted that the electronic structure of the vacuum/oxide interface is not important in practical device since the oxide would have a gate metal on the top surface. To fix the problem of Al under-coordination at the oxide/vacuum interface, 8 OH groups have been added so that every Al at the oxide/vacuum interface was bonded to at least 4 O atoms. To avoid significant interface deformation, these 8 OH groups have been added in two steps: 4 OH's were added and the whole system was relaxed, then 4 more OH's were added, and the whole system was relaxed. This led to a-Al$_2$O$_3$/InGaAs interface without significant changes in interfacial geometry, but passivated the upper oxide–vacuum interface.

The high-temperature (1100 K) annealing of the a-Al$_2$O$_3$/In$_{0.5}$Ga$_{0.5}$As interface of the one-interface design resulted in complete interface delamination indicating generally weak oxide–semiconductor interfacial bonding. This delamination led to a complete breaking of oxide–semiconductor bonds, physical separation of oxide and semiconductor slabs with no signs of intermixing, and partial relaxation of oxide/vacuum and semiconductor/vacuum interfaces making them more chemically-passive. The bonding be-

Fig. 3. a-Al$_2$O$_3$/InAlAs/InGaAs stack after final relaxation.

layer-by-layer substrate deformation in the annealed–cooled–re-laxed oxide/semiconductor stack, we use the following norm: $\Delta \bar{R}_i = \frac{1}{N_i} \sum_j |\bar{R}_j - \bar{R}_{0j}|$, where N_i is the number of atoms in horizontal layer i, $\bar{R}_j$ and $\bar{R}_{0j}$ are coordinates of atom j belonging to the horizontal layer i after the interface relaxation and in the initial relaxed clean substrate slab, while index j goes along every substrate atom in horizontal layer i.

The a-Al_2O_3/Ge interface demonstrates significant intermixing and substrate deformation for both annealing temperatures (700 K and 1100 K). The distortion of the Ge surface by a-Al_2O_3 creates vacancies which facilitate O interdiffusion. For the 700 K annealed a-Al_2O_3/Ge interface, the average substrate deviations quantified by layer-by-layer norm $\Delta \bar{R}_i$ are 2.4 Å, 1.3 Å, 0.9 Å and 0.2 Å for the Ge layers starting with the uppermost and down into the Ge bulk (EPAPS Fig. 2). The Ge slabs used in these models have 8 atoms per layer. The three bottom Ge layers demonstrate zero deviation since they are fixed in the bulk locations. The corresponding Ge deviations for the 1000 K annealed interface are 1.5 Å, 1.7 Å, 1.2 Å, and 0.5 Å (EPAPS Fig. 2). The increasing of annealing temperature leads to substantially greater deformation in Ge substrate (Fig. 1a and b) and micro-cavity formation in a-Al_2O_3 oxide.

The a-Al_2O_3/InGaAs interface demonstrates practically no inter-mixing both for one-interface (Fig. 2) and two-interface models (Fig. 1 EPAPS). There are only small displacements of InGaAs inter-face atoms and low InGaAs lattice distortion relative to the atomic positions in the InGaAs prior to oxide bonding (Fig. 2). For the one-interface a-Al_2O_3/InGaAs design (Fig. 2), the average deviations per layer are 0.56 Å, 0.56 Å, 0.19 Å, and 0.09 Å starting with the upper-most row half-layer and moving layer-by-layer down into the InGaAs bulk. There is no deviation of the substrate bottom three layers since they are fixed in bulk positions. The deviations for InGaAs surface layers in the 800 K annealed a-Al_2O_3/InGaAs stack are much less (2× to 5×) than for Ge layers in the 700 K annealed a-Al_2O_3/Ge interfaces indicating that the a-Al_2O_3/InGaAs interface produces much less substrate distortion than a-Al_2O_3/Ge (EPAPS Fig. 2).

The a-Al_2O_3/InAlAs interface of the a-Al_2O_3/InAlAs/InGaAs stack demonstrates medium intermixing with an Al atom pulled from the InAlAs row into the oxide creating a metal–metal Al–In bond (Fig. 3). The deformation estimated as average deviation per layer by metric $\Delta \bar{R}_i$ gives 1.04 Å, 0.44 Å, 0.19 Å, and 0.12 Å starting with the uppermost row half-layer and moving layer-by-layer down into the InAlAs bulk (EPAPS Fig. 2).

Comparative analysis of the substrate deformation in interface region for all three oxide–semiconductor systems (Figs. 1–3) clearly indicates that the largest deformation and intermixing are found in a-Al_2O_3/Ge interfaces (both for 700 K and 1100 K). The a-Al_2O_3/InAlAs interface demonstrates medium deformation and intermixing, while a-Al_2O_3/InGaAs has lowest interface deforma-tion and practically no intermixing (EPAPS Fig. 2). The fact that a-Al_2O_3/InGaAs interface has generally weak interface bonding, no intermixing and very limited deformation at 800 K annealing temperature indicates that a-Al_2O_3/InGaAs is the most promising interface among the three investigated.

6.3. Bader charge analysis

Interfacial bonding can result in a strong interface polarity, which is undesirable since significant charge transfer can have a negative impact on device performance. To quantify this effect, a Bader charge analysis was performed [30,31]. For the a-Al_2O_3/Ge interfaces annealed at 700 K and 1100 K, the Bader charge analysis indicates that the Ge atoms bonded to O lose, on average, about 0.7–1.0 |e| of atomic charge relative to the clean Ge(1 0 0)(2 × 1) surface (Fig. 1). For comparison to XPS data, the Bader charge of

the interfacial atoms relative to bulk semiconductor and oxide atoms were calculated. The Bader charge of interface Ge atoms with respect to the bulk Ge atoms shows mild Bader charge deple-tion of 0.3–0.7 |e|. The analysis of oxide atoms at the interface shows that relative to the oxide bulk atoms, the O atoms bonded to Ge are depleted by 0.15–0.30 |e|, while Al atoms bonded to interface O have near bulk Bader charge values. The total charge transfer from the Ge substrate into the a-Al_2O_3 bulk through the semiconductor/oxide interface was calculated from the total Bader atomic charge summed up over all Ge atoms and bottom passivat-ing H's in the a-Al_2O_3/Ge system and comparing it with the same total charge summed up over the clean vacuum/semiconductor Ge(1 0 0)(2 × 1) slab with bottom passivating H atoms. This total charge transfer analysis demonstrated that the 700 K annealed interface depleted the Ge substrate by 9.23 |e| of charge, corre-sponding to a normalized charge transfer of -6.88×10^{-2} |e|/Å² (Fig. 1a). The 1100 K annealed a-Al_2O_3/Ge interface depleted the Ge substrate of 9.12 |e| resulting in -6.80×10^{-2} |e|/Å² of normal-ized charge transfer (Fig. 1b).

The Bader charge analysis for the a-Al_2O_3/InGaAs interface (Fig. 2) indicated that relative to the clean $In_{0.5}Ga_{0.5}As$(1 0 0)-(4 × 2) surface atoms, the As atoms bonded to Al gained ~0.4 |e|, the In and Ga bonded to one O atom lost ~0.3 |e|, while In bonded to two O atoms lost ~0.7 |e|. These results show weakly polar bond formation and no ionic bonding. Relative to bulk atoms, the As bonded to Al have excessive charge of ~0.26 |e|, the In bonded to one O atom are depleted by ~0.18 |e|, the In bonded to two O's are depleted by ~0.40 |e|, and the Ga bonded to one O are depleted by ~0.08 |e|. Interfacial semiconductor atoms in an unpinned inter-face should have near bulk-like charge. The analysis of the inter-face oxide atoms indicates that O bonded to In or Ga is depleted by 0.12–0.17 |e| and Al bonded to As has a mild Bader charge gain of 0.0–0.2 |e| versus O and Al atoms in bulk a-Al_2O_3. The interfacial O, an electron acceptor, is depleted of electrons relative to bulk oxide because the O–Al bonds are switched to O–In/Ga bonds, so oxygen switches to bonding to a more electronegative (less elec-tropositive) atom. Conversely, Al, an electron donor, gains elec-trons because the Al–O bonds are switched to Al–As bonds, so Al switches to bonding to a less electronegative atom. The quantita-tive analysis of the total charge transfer through a-Al_2O_3/InGaAs interface indicated that after stacking to a-Al_2O_3 the InGaAs slab was depleted by ~1.23 |e| with limited -8.6×10^{-3} |e|/Å² of nor-malized charge transfer consistent with a good interface for micro-electronics applications.

The Bader charge analysis for a-Al_2O_3/InAlAs interface of the a-Al_2O_3/InAlAs/InGaAs stack (Fig. 3) indicated that relative to the clean $In_{0.5}Al_{0.5}As$(1 0 0)-(4 × 2) surface atoms, the As atoms bonded to oxide Al gained ~0.8 |e|, the In atoms bonded to single oxide Al gained ~0.3 |e|, and the In atoms bonded to single O lost ~0.06–0.09 |e|. The semiconductor Al atoms bonded to single O lost ~0.4–1.1 |e|, while the substrate Al atom pulled into the oxide and bonded to two O atoms and one In lost ~0.2 |e|. Relative to In-AlAs bulk atoms, the semiconductor Al bonded to O are depleted by ~0.02–0.20 |e|, the In atoms bonded to oxide Al or O gain ~0.3 |e| (in bulk In is bonded to four As), and As atoms bonded to oxide Al gain ~0.0–0.3 |e|. The oxide Bader charge analysis shows that interface O atoms differ by −0.11–0.0 |e| and oxide Al by +0.1 |e| Bader charges from in-bulk oxide atoms. The total charge transfer analysis demonstrates that the a-Al_2O_3/InAlAs interface depletes the InAlAs/InGaAs substrate by ~1.55 |e| of charge corresponding to a normalized charge transfer of -1.08×10^{-2} |e|/Å² (Fig. 3). This medium interfacial charge transfer would lead to interface dipole creation and a negative effect on the a-Al_2O_3/InAlAs interface per-formance in a-Al_2O_3/InAlAs/InGaAs stacks. It is noted that the small changes in Bader charge even for the substrate atoms pulled into the bulk indicated that XPS chemical shifts cannot always be used

to determine the extent of interface intermixing of amorphous oxide/compound semiconductor interfaces.

The comparative analysis of all three investigated interfaces indicates that the a-Al$_2$O$_3$/InGaAs demonstrates the lowest absolute charge transfer through the interface (-8.6×10^{-3} |e|/Å^2), while a-Al$_2$O$_3$/Ge (700 K, 1100 K) interfaces have around ~8 times higher absolute values of -6.8×10^{-2}, and the charge transfer through the a-Al$_2$O$_3$/InAlAs interface is -1.08×10^{-2} |e|/Å^2 or ~1.3 times higher in absolute value than in a-Al$_2$O$_3$/InGaAs.

6.4. Coordination analysis

The interfacial coordination number distribution has a significant impact on electronic properties and interface performance in microelectronic devices. For example, changes in coordination number can generate partially filled dangling bonds which pin the Fermi level. To understand how the semiconductor and a-Al$_2$O$_3$ oxide structures are altered by mutual bonding, the changes in semiconductor and a-Al$_2$O$_3$ surface coordinations were investigated and compared for the a-Al$_2$O$_3$/Ge, a-Al$_2$O$_3$/InAlAs/InGaAs and a-Al$_2$O$_3$/InGaAs interfaces. In computer simulations, the "coordination" value is determined by the number of nearest neighbors within a certain cutoff radius; this can create small difference in coordination number distributions in comparison with a direct imaging of electron density. The coordination numbers were determined using bond building algorithms implemented in Accelrys Materials Studio based on large database of atomic configurations, and, in addition, they were verified by using empirical atomic radii values, evaluating bond cutoff as $R_{cut} = k * (R_1 + R_2)$, ($k = 1.1$). Below, the coordination numbers of the surface atoms at the vaccum/a-Al$_2$O$_3$, vacuum/semiconductor, and a-Al$_2$O$_3$/semiconductor interfaces are compared.

The stacking of a-Al$_2$O$_3$ onto Ge(1 0 0)(2 × 1) reconstruction (Fig. 1) significantly perturbs the Ge substrate coordination distribution. For the 700 K annealing case (Fig. 1a), Ge atom coordination switches from 100% 3-fold coordination at the vacuum interface to 45% 3- and 4-fold coordination and 10% 2-fold coordination. A few Ge atoms are pulled out of the substrate and are bonded only to O atoms resulting in 2-fold coordinated Ge atoms. Ge atoms which do not form bonds to the oxide preserve the original 3-fold coordination. The high-temperature annealed interface (1100 K, Fig. 1b) has only minor deviations in coordination distribution of Ge in comparison with the 700 K annealed case (Fig. 1a) leading to an equal partition of 3- and 4-coordinated Ge atoms with no 2-fold coordinated ones. The largest changes in coordination are consistent with strong a-Al$_2$O$_3$/Ge(1 0 0)(2 × 1) bonding and intermixing.

The In$_{0.5}$Ga$_{0.5}$As(1 0 0)-(4 × 2) vacuum/semiconductor interface has a row and trough structure with different atomic coordinations. The row coordination is 3-fold As, 2-fold In, and 2-fold Ga atoms. After stacking to a-Al$_2$O$_3$, 75% of As atoms in the row preserve 3-fold coordination while 25% switch to 4-fold coordination. The Ga atoms in the row preserve 2-fold coordination after stacking, while the In increase coordination from 2- to 4-fold. The Ga atoms in the trough have 3-fold coordination for the vacuum/InGaAs interface and preserve it after stacking to a-Al$_2$O$_3$, while In switches from 3-fold coordination (for the vacuum/semiconductor interface) to the 4-fold coordination for the oxide/semiconductor interface. The small changes in coordination are consistent with very weak a-Al$_2$O$_3$/In$_{0.5}$Ga$_{0.5}$As(1 0 0)-(4 × 2) bonding.

The In$_{0.5}$Al$_{0.5}$As(1 0 0)-(4 × 2) vacuum/semiconductor interface has a row and trough structure with different atomic coordinations. The row coordination is 3-fold As, 2-fold In, and 2-fold coordinated Al atoms. After stacking to a-Al$_2$O$_3$, 75% of As atoms in the row preserve 3-fold coordination while the remaining 25% get 2-fold coordination. After bonding to oxide, the Al atoms in the

row increase their coordination from 2- to 4-fold, while In atoms increase their coordination from 2- to 3-fold. For the vacuum/InAlAs(1 0 0)-(4 × 2) interface, the Al atoms in a trough have 3-coordination, and the stacking to a-Al$_2$O$_3$ increases it to equally partitioned 3- and 4-fold coordination, while In switches from 3-fold coordination to the equally partitioned 3- and 4-fold coordination for the oxide/semiconductor interface. The large changes in coordination are consistent with strong a-Al$_2$O$_3$/In$_{0.5}$Al$_{0.5}$As(1 0 0)-(4 × 2) bonding and intermixing.

The effect of oxide bonding was described on the coordination of the substrate atoms; below, the effect of substrate bonding on the coordination of the oxide atoms is described. The coordination of the interfacial oxide atoms is compared to both bulk oxide coordination and coordination at vacuum/oxide interfaces. Previous DFT-MD simulations of a-Al$_2$O$_3$ vacuum/oxide interface reported surface oxygen enrichment with a roughly equal partition of 2- and 3-coordinated surface oxygen atoms, while the Al atoms closest to the surface which form bonds to surface O atoms had ~15% of 3-fold, ~75% of 4-fold and ~10% of 5-fold coordinated atoms [8].

The oxygen atoms in the a-Al$_2$O$_3$/Ge interface region for both annealing temperatures have nearly identical total coordination numbers (i.e. O–Al plus O–Ge) as the oxygen at the vacuum/oxide a-Al$_2$O$_3$ surface: roughly equal partition of 2- and 3-fold coordinated oxygens. A few O atoms diffuse into subsurface Ge to form 2 bonds to Ge atoms breaking Ge–Ge bonds. Since the Al atoms do not make bonds to the Ge substrate, the Al atoms closest to the a-Al$_2$O$_3$/Ge interface preserve the same coordination distribution of subsurface Al atoms as at the a-Al$_2$O$_3$/vacuum interface.

Conversely, the stacking of a-Al$_2$O$_3$ to InGaAs (Fig. 2) changes interface coordination of the oxide atoms resulting in 3-fold coordination for all interface O atoms, while interface Al atoms slightly lower their coordination to ~10% 3-fold and ~90% 4-fold coordination These small changes in Al coordination are considered insignificant because of the small number of atoms in the model structure. DFT-MD simulations due to their high computational cost preclude employing large ensembles; therefore, the present coordination partitions should be considered as estimates. This is consistent with Al at the semiconductor interface bonding via substituting an Al–O bond for an Al–As bond while O atoms at the semiconductor interface bond by forming a new O–In or O–Ga bond while usually retaining all their O–Al bonds.

Similar to the previous case, the stacking of a-Al$_2$O$_3$ to InAlAs(1 0 0)-(4 × 2) (Fig. 3) changes interface coordination of the oxide atoms resulting in 3-fold coordination for all interface O atoms, while interface oxide Al atoms slightly increase their coordination to ~80% 4-fold and ~20% for 5-fold.

The a-Al$_2$O$_3$/Ge interface demonstrates a bonding model different from the a-Al$_2$O$_3$/InAlAs and a-Al$_2$O$_3$/InGaAs interfaces. The vacuum/a-Al$_2$O$_3$ interface has pronounced oxygen enrichment, which is preserved in the a-Al$_2$O$_3$/Ge interface, where bonding is formed exclusively by Al–O–Ge bonds. Conversely, a-Al$_2$O$_3$/InAlAs and a-Al$_2$O$_3$/InGaAs interfaces do not demonstrate such oxygen enrichment, having both O and Al bonded to the semiconductor.

6.5. Density of state analysis

To investigate electronic structure of the interfaces, Density of States (DOS) curves were calculated for the interface regions, semiconductor layers below interfaces corresponding to conduction channels, and clean substrates without oxide (Fig. 4).

For the a-Al$_2$O$_3$/Ge interface (Fig. 1), the standard DFT DOS calculations can not provide detailed information about electronic structure, since standard DFT due to band gap underestimation only has a density of states minimum at the Fermi level instead
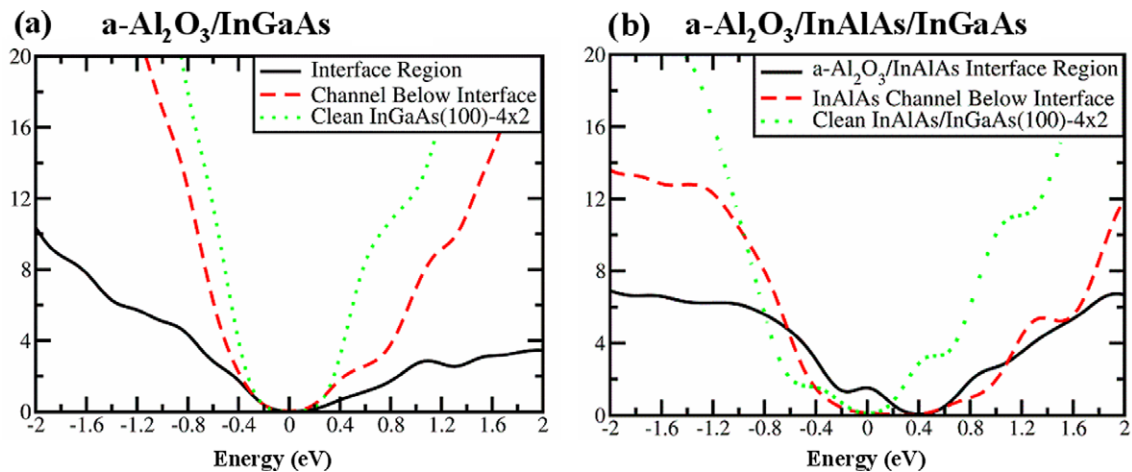
Fig. 4. Density of states for a-Al$_2$O$_3$/InGaAs and a-Al$_2$O$_3$/InAlAs/InGaAs stacks. The Fermi level is at 0.0 eV.

of a bandgap for Ge. However, the comparison of calculated DOS curves for both annealing temperatures (700 K and 1100 K) indicates that formation of interface with a-Al$_2$O$_3$ creates increased density of states at $E_f = 0$ in the interface region in comparison with the clean Ge(1 0 0)(2 × 1) substrate. This can indicate that the interface is pinned due to the interface intermixing, coordination perturbations and dangling bonds on Ge atoms non-bonded to the oxide (Fig. 1).

The DOS curves for the clean InGaAs(1 0 0)-(4 × 2) slab and a-Al$_2$O$_3$/InGaAs are compared in Fig. 4-a; for a-Al$_2$O$_3$/InGaAs, both the DOS of the a-Al$_2$O$_3$/InGaAs interface and InGaAs channel below interface are shown. The simulated DFT band gaps for InGaAs are lower in value than the experimental ones due to the standard DFT band gap underestimation coming from approximated nature of exchange interaction. For a-Al$_2$O$_3$/InGaAs, the Fermi level is positioned in the middle of the band gap region. The DFT-MD simulations of a-Al$_2$O$_3$/InGaAs stack indicated a weak interface bonding consistent with both the low density of bonds and the simulated delamination at 1100 K. The calculated DOS demonstrates no significant DOS changes near the band gap region nor electronic structure perturbation after the interface formation. This result is consistent with the hypothesis than an unpinned interfaces can be formed if the interaction between the highly ionic metal oxide and semiconductor channel is weak similar to observations for gate oxides on carbon nanotubes [32].

The DOS curves for the clean InAlAs/InGaAs slab and a-Al$_2$O$_3$/InAlAs interface are compared in Fig. 4-b; for a-Al$_2$O$_3$/InAlAs, both the DOS of the a-Al$_2$O$_3$/InAlAs interface and InAlAs channel below interface are shown. The comparison of the DOS curves for InAlAs channel and a-Al$_2$O$_3$/InAlAs interface shows that the interface gains additional states near the bandgap region edges. These states can be result of interface intermixing; the simulations show that substrate Al atoms were pulled into the oxide creating In–Al metal–metal bonds (Fig. 3). To investigate these newly created band gap edge states, the band-decomposed charge density corresponding to the energy interval of −0.2 eV to 0.2 eV (Fig. 4) was visualized in 3D. It confirmed that the states corresponding to this energy interval are dangling bonds localized on two interfacial As atoms in InAlAs row which were previously bonded to the substrate Al atom pulled into the oxide. In typical experiments with much longer annealing timescales, this intermixing would probably be more extensive. It is noted that this interface is pinned due to intermixing creating dangling bonds instead of large changes in the charge state of the interface atoms due to ionic bonding alone.

6.6. Comparison to experimental data

Direct comparison between DFT-MD simulations of oxide–semiconductor interfaces and experimental measurements is not straightforward since computer simulations often consider ideal cases while experimental measurements introduce deviations from ideal situation due to sample preparation and oxide growth processing. In addition, DFT-MD simulations due to their high computational cost usually limit the system size to several hundred atoms and time-length to several picoseconds. Nevertheless, results of our DFT-MD simulations demonstrate good correlation to experimental measurements reproducing major physico-chemical interface phenomena.

6.6.1. a-Al$_2$O$_3$/Ge(1 0 0)(2 × 1)
Unlike silicon, annealing of high-k/Ge interfaces does not result in interlayer oxide formation [33,34]; therefore, interlayer oxide formation on Ge is specific to the oxide deposition technique. The three common gate oxide deposition methods are (a) atomic layer deposition (ALD) or metal organic chemical vapor deposition (MOCVD); (b) sputter deposition; (c) oxidation of a metal film. Most studies employed a GeO$_2$ or GeON [35–38] passivation layer. The effect of a passivation layer on interfacial bonding and electronic structure between an amorphous oxide and Ge(1 0 0) will be addressed in a future paper. Due to the thermal instability and low dielectric constant of GeO$_2$, it is desirable to directly bond oxide to Ge using either sputter or electron beam deposition techniques [39]. Electron beam oxide deposition is employed for gate oxide formation on Ge using two methods. (i) An oxide can be directly evaporated by an electron beam. Nearly all oxides evaporate incongruently resulting in O$_2$ generation; the O$_2$ can react with Ge disrupting the lattice. (ii) A thin metal such as Hf or Zr is deposited at low temperature on Ge and oxidized using ozone [40]. Since the metal is more reactive to O$_3$ than Ge and metal oxides are reasonably good diffusion barriers, this can result in the formation of the abrupt oxide/Ge interface.

Data from two studies are consistent with the DFT-MD results for Al$_2$O$_3$/Ge(1 0 0): (1) Malasfsky studied the deposition of Ge on crystalline Al$_2$O$_3$ [41]. The Ge forms crystalline clusters producing an interface similar to the one in the DFT-MD studies. For sub-monolayer coverages, Ge is observed by XPS in the Ge^{+4} oxidation state consistent with bonding selectively to oxygen atoms on the Al$_2$O$_3$ surface consistent with the DFT-MD results. For all coverages, the Al and O peaks are bulk-like consistent with the small shifts in charge calculated with the DFT-MD simulations. For Ge

coverages above 2ML, the XPS spectrum consists almost entirely of Ge in Ge^{+0} consistent with the small shifts in charge calculated with the DFT-MD simulations. (2) Bellenger et al. studied the formation of a-Al$_2$O$_3$/Ge using Al evaporation onto Ge(1 0 0) in the presence of atomic oxygen [42]. TEM images show an amorphous oxide with an abrupt interface to Ge without an obvious interlayer. XPS studies show the Al peak is unshifted compared to that from Al$_2$O$_3$ consistent with the charge changes calculated with DFT-MD. The Ge XPS spectrum shows a small amount of Ge^{+2}, Ge^{+3}, and Ge^{+4} consistent with Ge–O bonds over a region of less than 8 Angstroms. This experimentally observed intermixing is greater than the experimentally observed intermixing for ZrO$_2$/Ge(1 0 0)-(2 × 1)[43–45] consistent with the DFT-MD calculations [7,8]. However, Bellinger et al. simultaneously exposed the surface to Al and O atoms which would tend to place a bit more oxygen at the interface than oxidation of a Al film so the comparison to a-ZrO$_2$/Ge interfaces cited above is slightly biased.

6.6.2. a-Al$_2$O$_3$/InAlAs

The literature on the bonding of a-Al$_2$O$_3$ to any aluminum containing semiconductor is sparse. However, Yasuda et al. have performed a comparison of the interfaces for ALD grown a-Al$_2$O$_3$ on GaAs(1 0 0), In$_{0.53}$Ga$_{0.47}$As(1 0 0), In$_{0.52}$Al$_{0.48}$As, and Al$_{0.5}$Ga$_{0.5}$As [46]. The samples were wet cleaned in NH$_3$ solution prior to ALD. The best C–V characteristics (modest frequency dispersion and low hysteresis) were obtained on the InGaAs samples which have a small bandgap (0.8 eV). Significantly higher dispersion and hysteresis was observed for both GaAs(1 0 0) and In$_{0.52}$Al$_{0.48}$As which have comparable bandgaps (1.4 eV) while almost no capacitance modulation was observed for Al$_{0.5}$Ga$_{0.5}$As which has a large bandgap (2.0 eV). Yasuda et al. compared the bulk-like and oxide-like XPS peaks of In, Ga, and As after a-Al$_2$O$_3$ ALD to determine the amount of residual substrate oxide and the formation of new substrate oxide due to the ALD. They observed that the amount of post ALD As oxide was 6x greater on InAlAs(1 0 0) than on InGaAs (1 0 0), but the differences in post ALD In/Ga oxides were modest. Some of the difference in the amount of In/Ga post ALD oxides between the InGaAs(1 0 0) and InAlAs(1 0 0) reflects the difference in preexisting oxide on the surface prior to ALD so it is difficult to make an precise comparison to the DFT-MD simulation which assume a clean starting surface. A recent study on HfO$_2$ ALD on InGaAs vs InAlAs also shows the enhanced intermixing for oxide on Al containing semiconductors [47]. However, the experimental data is consistent with the lack of intermixing and nearly bulk-like interfacial charge states for a-Al$_2$O$_3$/InGaAs(1 0 0) in contrast to a-Al$_2$O$_3$/InAlAs(1 0 0) for which intermixing is predicted.

6.6.3. a-Al$_2$O$_3$/InGaAs

The bonding structure of a-Al$_2$O$_3$ on In$_{0.2}$Ga$_{0.8}$As has been studied with in situ monochromatic XPS (peak position accuracy ±0.05 eV) for ALD a-Al$_2$O$_3$ to determine the chemical shift with great accuracy by Milojevic et al. [48]. The samples were wet cleaned in NH$_4$S, and trimethyl aluminum was employed to reduce the residual surface oxides; this process (ALD cleanup) is effective at 300 °C but still leaves some gallium oxides. For XPS of oxide–semiconductor interfaces, the reference states of the semiconductor and oxide atoms are the bulk semiconductor and oxide atoms; for example, InGaAs would be assigned as In^{+0}, Ga^{+0}, and As^{+0} while Al$_2$O$_3$ would be assigned as Al^{+3} and O^{-2}. The TMA reduces the Ga$_2$O$_3$, but a Ga^{+1} peak remains consistent with either residual sulfur at the interface or Ga–O bonding [49]. The As being in a As^{+0} state is consistent with the absence of arsenic oxides. The aluminum peak is consistent with Al only being in an O–Al–O bonding environment. In a recent report, Milojevic et al. were able to resolve the Ga^{+1} from GaO$_x$ from Ga–S bonding states [50]. They found that neither Ga^{+1} from GaO$_x$ nor Ga–S are removed by

ALD; conversely, they did find that all arsenic sulfide species are removed by ALD. A related experiment was performed by Aguirre-Tostado et al. on samples for which atomic hydrogen was employed to remove native oxides instead the NH$_4$S wet clean [51]. Again a Ga^{+1} XPS peak was found at the interface was assigned to Ga–O bonding since no sulfur was present. This remaining Ga–O at the interface can be ascribed to either residual substrate oxides or bonding between the a-Al$_2$O$_3$ and the substrate. However, the atomic hydrogen cleaning does deplete the surface of In and creates As–As bonds so the surface is not exactly comparable to the one in the present DFT study. However, these experiments are consistent with the DFT-MD simulations predicting that the bonding between a-Al$_2$O$_3$ and InGaAs being sufficiently weak that the As, Al, and O charge states are bulk-like and the Ga is slightly shifted due to the loss of a partial charge.

The cleanest a-Al$_2$O$_3$/In$_{0.53}$Ga$_{0.47}$As(1 0 0) interfaces are prepared by in situ decapping of As$_2$-capped In$_{0.53}$Ga$_{0.47}$As(1 0 0) followed by a-Al$_2$O$_3$ ALD [52,53]. Using this technique, Kim et al. have observed a chemically abrupt interface using high resolution TEM; high-angle annular dark-field (HAADF) TEM also showed no interfacial oxide formation. Angle resolved XPS spectra showed the complete absence of any chemical shift of the interfacial Ga, In, and As atoms. It is noted that this XPS spectrometer has lower resolution than the one employed by Shahrjerdi et al. so a small chemical shift may still be present [49]. The data are consistent with the DFT-MD simulations showing that the bonding between a-Al$_2$O$_3$ and InGaAs(1 0 0) is weak and nearly covalent with chemical shifts of less than one electron for all the interfacial atoms.

The abruptness of an oxide–semiconductor interface can be observed by transmission electron microscopy (TEM). Cheng and Fitzgerald prepared very clean a-Al$_2$O$_3$/GaAs interfaces by using MOCVD to both grow GaAs and a-Al$_2$O$_3$ in the same chamber [54]. It is noted that the a-Al$_2$O$_3$ was grown on an As-rich surface at 370 °C while the DFT simulations are for bonding on the In/Ga rich InGaAs(1 0 0)-(4 × 2) surface since it is expected to be more stable in the presence of oxidant. TEM images reveal a completely abrupt interface, and XPS shows the absence of any arsenic oxides. Similar TEM results have been observed by Shahrjerdi et al. and by Hong-Liang for ALD deposited a-Al$_2$O$_3$ on HF cleaned GaAs(1 0 0) [49,55]. Although the DFT-MD simulation were for a-Al$_2$O$_3$/In$_{0.5}$Ga$_{0.5}$As(1 0 0) and these experiments were performed on GaAs(1 0 0), the interfacial chemistry is similar. Furthermore, Huang et al. reported HRTEM measurements of ALD grown a-Al$_2$O$_3$ on wet cleaned InGaAs revealing a sharp interface between the oxide and the semiconductor both for stacks as-deposited and annealed in nitrogen at 500 °C [56]. In addition, C–V measurements of Al$_2$O$_3$/In$_{0.53}$Ga$_{0.47}$As stacks formed by in situ decapping indicated strong inversion at elevated temperatures, consistent with an unpinned Al$_2$O$_3$/InGaAs interface [52,53], correlating with the DFT-MD DOS calculations (Fig. 4).

Transistor device results from Xuan et al. for a-Al$_2$O$_3$/InGaAs prepared by wet cleaning of the substrate, show very high output current, low threshold voltages, reasonable subthreshold slopes, and reasonably low off current for submicron devices [57]. For In$_{0.65}$Ga$_{0.35}$As 400-nm channels enhancement mode devices, G_m(extrinsic, V_{DS} = 2 V) = 350 mS/mm, V_T = 0.4 V, SS = 350 mV/dec, and $I_{on}(V_{GS}$ = 4 V)/$I_{off}(V_{GS}$ = 0 V) = 150 in source current [57]. Although the subthreshold swing and I_{on}/I_{off} were modest, probably due to the non-optimized implanted source and drain, the output currents were high and scaled with gate length. Xuan et al. obtained better results with higher indium content devices [58]. For In$_{0.75}$Ga$_{0.25}$As 750-nm channel enhancement mode devices, G_m(extrinsic) = 430 mS/mm, V_T = 0.5 V, SS = 190 mV/dec, and $I_{on}(V_{GS}$ = 1 eV)/$I_{off}(V_{GS}$ = 0 V) = 10^6 in source current [58]. Again the modest subthreshold swing is ascribed to both problems associated with the implanted source drains instead of just interface

traps; therefore, the authors feel there is substantial room for improvement. Submicron devices had lower subthreshold swings consistent with this hypothesis, and $C–V$ analysis showed a $D_{it} = 8 \times 10^{11}/cm^2$-eV using the Terman method [58]. These results are consistent with a modest density of states at the interface throughout most of the bandgap as predicted by the DFT DOS presented in this manuscript (Fig. 4). It is noted that even better device results might be obtained using decapped samples and in situ oxide deposition after heterostructure growth since the studies cited above show wet cleaning leaves some gallium oxides/sulfites which are likely to create some interface states and UHV MBE deposited oxides on in situ regrown semiconductor surfaces have the lowest reported subthreshold swings [59].

6.7. Qualitative comparison of interface bonding

The most general observations from the DFT-MD calculations are (a) the a-Al_2O_3/InGaAs interface is more stable than the a-Al_2O_3/InAlAs interface, (b) the a-Al_2O_3/InGaAs interface has a good electronic structure, (c) the a-Al_2O_3/InGaAs interface has O–Ga and O–In and no O–As bonds, and (d) the a-Al_2O_3/InGaAs interface has less substrate distortion than the a-Al_2O_3/Ge interface. The first three observations can readily be rationalized by the strengths of the oxide and interfacial bonds. The bonds strengths of the oxides are estimated based on the Gibbs free energy per mole of oxygen atoms. A similar technique could be used for formation of arsenic oxide, but its Gibbs free energy is so low, it does not need to be considered in detail.

$$1/2Ge(s) + 1/3Al_2O_3(s) \rightarrow 1/2GeO_2(s) + 2/3Al(s)$$

$$4/3In_{0.5}Ga_{0.5}As(s) + 1/3Al_2O_3(s) \rightarrow 1/3Ga_2O_3(s) \\ + 4/3In_{0.5}Al_{0.5}As(s)$$

$$4/3In_{0.5}Ga_{0.5}As(s) + 1/3Al_2O_3(s) \rightarrow 1/3In_2O_3(s) \\ + 4/3Ga_{0.5}Al_{0.5}As(s)$$

$$2/5In_{0.5}Ga_{0.5}As(s) + 1/3Al_2O_3(s) \rightarrow 1/5As_2O_5(s) + 1/5In(s) \\ + 1/5Ga(s) + 2/3Al(s)$$
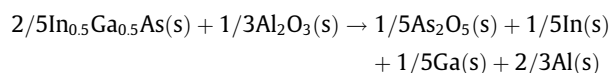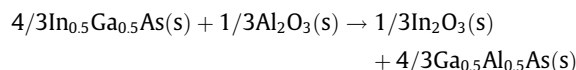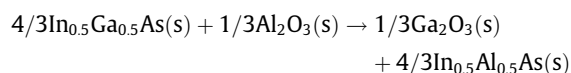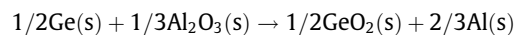
To simplify the estimate, the thermodynamic values for the crystalline oxides are used instead of the amorphous ones, and it is assumed that all III-As semiconductors have the same free energy. Using these assumptions, the absolute Gibbs free energies per mole of O atoms are [60].

$$Al_2O_3(527\ kJ) \gg Ga_2O_3(333\ kJ) > In_2O_3(277\ kJ) > GeO_2(261\ kJ) \\ \gg As_2O_5(156\ kJ)$$
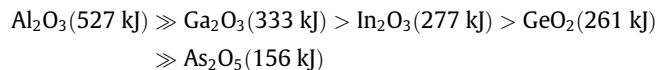
These Gibbs free energies can explain the first three observations: (a) It is very thermodynamically unfavorable for Al_2O_3 to exchange any internal bonds in order to intermix with InGaAs or Ge, but intermixing with InAlAs is more likely since Al incorporation into the oxide does not involve the loss of any Al–O bonds. (b) Since the internal bonds in Al_2O_3 are nearly twice as strong as any interfacial bonds, the bonding between Al_2O_3 and InGaAs is weak creating a good interfacial electronic structure. For Al_2O_3/Ge, the bonding is also weak, but the dangling bonds on Ge tend to be half-filled and create midgap states. (c) In the a-Al_2O_3/InGaAs interface O is bonded only to Ga and In atoms having no O-As bonds because the ionic bond strength is much greater for Ga_2O_3 and In_2O_3 than for As_2O_5. (d) The fourth observation, the lower distortion of the a-Al_2O_3/InGaAs interface vs. the a-Al_2O_3/Ge interface cannot be rationalized by thermodynamics. The bonds from oxygen in Al_2O_3 to Ge are weaker than the bonds from oxygen to In and Ga. The a-Al_2O_3/Ge interface has very few or no Al–Ge bonds

while the a-Al_2O_3/InGaAs interface has weak Al–As bonds. Therefore, simple thermodynamic trends cannot account for the lower distortion of the a-Al_2O_3/InGaAs. However, the kinetics of intermixing is very different for a-Al_2O_3/InGaAs and a-Al_2O_3/Ge. For a-Al_2O_3/InGaAs, the tri-coordinated surface atoms have nearly filled or empty dangling bonds since they are III–V atoms while for a-Al_2O_3/Ge, the tri-coordinated surface atoms have half-filled dangling bonds. Nearly filled or empty dangling bonds are analogous to the weakly reactive Lewis bases (NH_3) and acids (BH_3) while half-filled dangling bonds are analogous to highly reactive radicals (NO). Therefore, the distortion at the a-Al_2O_3/Ge interface is best explained by the highly reactive Ge surface forming a metastable bonding structure.

7. Conclusion

A comprehensive simulations of a-Al_2O_3/Ge, a-Al_2O_3/InGaAs, and a-Al_2O_3/InAlAs interfaces were performed with DFT-MD to investigate their structural and electronic properties on an atomic level. It was found that the a-Al_2O_3/Ge stacks annealed at 700 K and 1100 K create very rough interfaces with significant intermixing, interface charge transfer/dipoles, and many Ge dangling bonds. The a-Al_2O_3/InAlAs interface annealed at 800 K in the a-Al_2O_3/InAlAs/InGaAs stack has moderate intermixing with some Al atoms pulled out from the substrate into the oxide and moderate interface charge transfer/dipole. The a-Al_2O_3/InGaAs stack annealed at 800 K creates the best interface among the three investigated, demonstrating no intermixing, very low interface charge transfer/dipole, and consistent with unpinned Fermi level. The interface atoms demonstrate Bader charges very close to the in-bulk values consistent with XPS chemical shift data. From the simulation results, the best predictor of an unpinned interface between a highly ionic metal oxide and a compound semiconductor is weak bonding between the oxide and the semiconductor. In practice this can only be achieved if the deposition technique does not perturb the substrate and if the semiconductor surface has few partially filled dangling bonds since these are far more reactive than filled or empty dangling bonds.

Appendix A. Supplementary material

Supplementary data associated with this article can be found, in the online version, at doi:10.1016/j.susc.2009.08.009.

References

[1] G. Nicholas, T. Grasby, D. Lgoni, C. Beer, J. Parsons, M. Meuris, M. Heyns, IEEE Electron Device Letters 28 (2007) 825.
[2] S. Takagi, T. Tezuka, T. Irisawa, S. Nakaharai, T. Numata, K. Usuda, N. Sugiyama, M. Shichijo, R. Nakane, S. Sugahara, Solid-State Electronics 51 (2007) 526.
[3] K. Saraswat, C. Chui, T. Krishnamohan, D. Kim, A. Nayfeh, A. Pethe, Materials Science and Engineering B-Solid State Materials for Advanced Technology 135 (2006) 242.
[4] K. Tse, J. Robertson, Journal of Applied Physics 100 (2006) 093713.
[5] J. Ha, K. Seo, P. McIntyre, K. Sarawat, K. Cho, Applied Physics Letters 90 (2007) 112911.
[6] P. Broqvist, A. Pasquarello, Microelectronic Engineering 84 (2007) 2022.
[7] E. Chagarov, A. Kummel, Surface Science 602 (2008) L74.
[8] E. Chagarov, A. Kummel, Journal of Chemical Physics 130 (2009) 124717.
[9] P. Broqvist, A. Alkauskas, A. Pasquarello, Applied Physics Letters 92 (2008) 132911.
[10] E. Chagarov, A. Kummel, ECS Transactions 16 (2008) 773.
[11] G. Gutierrez, B. Johansson, Physical Review B 65 (2002) 104202.

[12] P. Lamparter, R. Kniep, Physica B 234 (1997) 405.
[13] H. Momida, T. Hamada, Y. Takagi, T. Yamamoto, T. Uda, T. Ohno, Physical Review B 73 (2006) 054108.
[14] S.M. Lee, D.G. Cahili, T.H. Allen, Physical Review B 52 (1995) 253.
[15] Y. Oka, T. Takahashi, K. Okada, S. Iwai, Journal of Non-Crystalline Solids 30 (1979) 349.
[16] S. Adiga, P. Zapol, L. Curtiss, Physical Review B 74 (2006) 064204.
[17] K. Shiraishi, Journal of the Physical Society of Japan 59 (1990) 3455.
[18] S. Plimpton, Journal of Computational Physics 117 (1995) 1.
[19] M. Matsui, Mineralogical Magazine 58A (1994) 571.
[20] G. Kresse, J. Furthmuller, Computational Materials Science 6 (1996) 15.
[21] G. Kresse, J. Furthmuller, Physical Review B 54 (1996) 11169.
[22] Blöchl, Physical Review B 50 (1994) 17953.
[23] G. Kresse, D. Joubert, Physical Review B 59 (1999) 1758.
[24] J. Perdew, K. Burke, M. Ernzerhof, Physical Review Letters 77 (1996) 3865.
[25] J. Perdew, K. Burke, M. Ernzerhof, Physical Review Letters 78 (1997) 1396.
[26] J. Neugebauer, M. Scheffler, Physical Review B 46 (1992) 16067.
[27] L. Alvarez, L. Leon, J. Sanz, M. Capitan, J. Odriozola, Physical Review B 50 (1994) 2561.
[28] C. Ruberto, Y. Yourdshahyan, B. Lundqvist, Physical Review B 67 (2003) 195412.
[29] D. Winn, M. Hale, T. Grassman, J. Sexton, A. Kummel, Journal of Chemical Physics 127 (2007) 134705.
[30] G. Henkelman, A. Arnaldsson, H. Jonsson, Computational Materials Science 36 (2006) 354.
[31] E. Sanville, S. Kenny, R. Smith, G. Henkelman, Journal of Computational Chemistry 28 (2007) 899.
[32] A. Javey, H. Kim, M. Brink, Q. Wang, A. Ural, J. Guo, P. McIntyre, P. McEuen, M. Lundstrom, H. Dai, Nature Materials 1 (2002) 241.
[33] C.O. Chui, H. Kim, D. Chi, P.C. McIntyre, K.C. Saraswat, IEEE Transactions on Electron Devices 53 (2006) 1509.
[34] Y. Kamata, Y. Kamimata, T. Ino, A. Nishiyama, Japanese Journal of Applied Physics B 44 (2005) 2323.
[35] S. Van Elshocht et al., Applied Physics Letters 85 (2004) 3824.
[36] K. Saraswat, D. Kim, T. Krishnamohan, D. Kuzum, A.K. Okyay, A. Pethe, H.-Y. Yu, ECS Transactions 16 (2008) 3.
[37] T. Tabata, C.H. Lee, K. Kita, A. Toriumi, ECS Transactions 16 (2008) 479.
[38] A. Delabie, F. Bellenger, M. Houssa, T. Conard, S.V. Elshocht, M. Caymax, M. Heyns, M. Meuris, Applied Physics Letters 91 (2008) 082904.
[39] Y. Abe, M. Miyata, T. Yasuda, ECS Transactions 16 (2008) 375.
[40] C.O. Chui, S. Ramanathan, B.B. Triplett, P.C. McIntyre, K.C. Saraswat, IEEE Electron Device Letters 25 (2002) 274.
[41] G. Malafsky, Surface Science 249 (1991) 159.
[42] F. Bellenger, C. Merckling, J. Penaud, M. Houssa, M. Caymax, M. Meuris, K. De Meyer, M.M. Heyns, ECS Transactions 16 (2008) 411.
[43] Y. Kamata, Y. Kamimuta, T. Ino, A. Nishiyama, Japanese Journal of Applied Physics Part 1-Regular Papers Brief Communications and Review Papers 44 (2005) 2323.
[44] C. Chui, D. Lee, A. Singh, P. Pianetta, K. Saraswat, Journal of Applied Physics 97 (2005) 113518.
[45] D. Chi, C.O. Chui, K.C. Saraswat, B.B. Triplett, P.C. McIntyre, Journal of Applied Physics 96 (2004) 813.
[46] T. Yasuda, N. Miyata, H. Ishii, T. Itatani, O. Ichikawa, N. Fukuhara, M. Hata, A. Ohtake, T. Haimoto, T. Hoshii, M. Takenaka, S. Takagi, Impact of Cation Composition and Surface Orientation on Electrical Properties of ALD-Al2O3/III-V Interfaces: As presented at the SISC 2008, San Diego, IEEE, 2008, p. 41.
[47] S. Oktyabrsky, V. Tokranov, S. Koveshnikov, M. Yakimov, R. Kambhampati, H. Bakhru, R. Moore, W. Tsai, Journal of Crystal Growth 12 (2009).
[48] M. Milojevic, F.S. Aguirre-Tostado, C.L. Hinkle, H.C. Kim, E.M. Vogel, J. Kim, R.M. Wallace, Applied Physics Letters 93 (2008) 202902.
[49] D. Shahrjerdi, D.I. Garcia-Gutierrez, E. Tutuc, S.K. Banerjee, Applied Physics Letters 92 (2008) 223501.
[50] M. Milojevic, F.S. Aguirre-Tostado, C.L. Hinkle, H.C. Kim, E.M. Vogel, J. Kim, R.M. Wallace, Applied Physics Letters 93 (2008) 252905.
[51] F.S. Aguirre-Tostado, M. Milojevic, B. Lee, J. Kim, R.M. Wallace, Applied Physics Letters 93 (2008) 172907.
[52] E. Kim, J. Cagnon, E. Chagarov, A.C. Kummel, K.C. Saraswat, S. Stemmer, P.C. McIntyre, Journal of Applied Physics, Submitted for publication.
[53] P.C. McIntyre, Y. Oshima, E. Kim, E. Chagarov, J. Cagnon, K.C. Saraswat, S. Stemmer, A.C. Kummel, Interface Studies of Metal Oxide Gate Insulators on Ge and III-V Substrates: As Presented at the SISC 2008, IEEE, San Diego, 2008.
[54] C.-W. Cheng, E.A. Fitzgerald, Applied Physics Letters 93 (2008) 031902.
[55] L. Hong-Liang, L. Yan-Bo, X. Min, D. Shi-Jin, S. Liang, Z. Wei, W. Li-Kang, Chinese Physics Letters 23 (2006) 1929.
[56] M. Huang, Y. Chang, C. Chang, Y. Lee, P. Chang, J. Kwo, T. Wu, M. Hong, Applied Physics Letters 87 (2005) 252104.
[57] Y. Xuan, Y.Q. Wu, P.D. Ye, Electron Device Letters 29 (2008) 294.
[58] Y. Xuan, T. Shen, M. Xu, Y.Q. Wu, P.D. Ye, High-Performance Surface Channel In-Rich $In_{0.75}Ga_{0.25}As$ Mosfets with ALD High-K As Gate Dielectric: IEDM 2008, San Fransisco, 2008, p. 371.
[59] R.J.W. Hill et al., IEEE Electron Device Letters 28 (2007) 1080.
[60] D.R. Lide (Ed.), CRC Handbook of Chemistry and Physics, CRC Press, 2007.